Microwave Radiation Imaging Using Inverse Synthetic Aperture Radar Technique

Steponas Ašmontas[1], Oleg Kiprijanovi [1], Boris Levitas[2], Jonas Matuzas[1, 2], Irina Naidionova[2]

[1]*Center for Physical Sciences and Technology,*
A. Goštauto 11, LT-01108, Vilnius, Lithuania
[2]*Geozondas JSC,*
Šev enkos 16, LT-03111, Vilnius, Lithuania
asmontas@pfi.lt

Abstract—Double-ridged horn antennas were used in ultra wideband radar system to create microwave radiation images. The images were obtained using inverse synthetic aperture radar technique. Transfer function of the calibrated radar system was close to one up to 22 GHz. High quality images of metallic and organic objects were created due to unique characteristic of ultra wideband radiated pulse. Metallic objects covered by visually opaque obstacles became detectable. The components of measurement set-up and the data processing are both important for the formation of these images.

The obtained results confirmed the ability of ultra wideband radar to form images for various practical applications including security systems. Higher frequency of such radar system can be raised up to 40 GHz-50 GHz.

Index Terms—ISAR technique, microwave radiation, double-ridged horn antenna, UWB pulses, UWB radar.

I. INTRODUCTION

The ability of microwave radiation to penetrate through a dielectric medium and atmosphere as well as better noise characteristics of receivers in this range compared with the infrared ones currently determines more intensive application of the microwaves for imaging [1]–[4]. Devices of microwave imaging find wide application in material characterization, in detection of hidden objects behind opaque materials and can serve as a powerful instrument in security systems.

The microwave imaging is achieved by using ultra wideband (UWB) radar system. Unique characteristics of the UWB microwave signal make it suitable for application in radar systems with high spatial resolution and obstacle penetration capabilities. The UWB signal is usually characterized by signal index y. In this work, index y represents relative frequency band and is expressed by

$$y = \left(f_{up} - f_{low} \right) / \left(f_{up} + f_{low} \right), \tag{1}$$

where f_{up}, f_{low} are the highest and the lowest frequencies of the signal spectrum, respectively. Signals with $y < 0.01$

belong to the narrow band, condition $0.01 < y < 0.25$ is attributed to the wide band, and the signals with $0.25 \le y < 1$ belong to the UWB signals [5].

In synthetic aperture radar (SAR) technique, the radar placed on a flying aircraft illuminates the standing object many times. Subsequent processing makes it equivalent to illumination of the object once but with longer synthesized aperture [6]. On the other hand, during the inverse synthetic aperture radar (ISAR) imaging the object is moving and the radar is stationary. ISAR measurements are usually used for radar imaging algorithm analysis and evaluation of object's reflection characteristics [7]. Recent creations of super wideband antennas and wideband digitized oscilloscopes have made the investigations of UWB signals easier. Both theoretical studies [8] and experimental research [9] keep uncovered new types of UWB signals. As it follows from analysis of the reviewed papers, the f_{up} of the UWB signals in the most cases was limited by the used experimental equipment, and therefore recent creation of digitized oscilloscopes, having passband up to 50 GHz, can reveal some unknown features of UWB signals.

In the UWB radar system we use modified double-ridged horn antennas [10]. Despite their sizes and narrow directional pattern their use in our radar system is preferred because they form UWB electromagnetic signal that remains irreplaceable for certain practical applications.

II. THEORETICAL BACKGROUND

ISAR image can be derived from electromagnetic plane wave integral – reflections from each point in the far field

$$E\left(\vec{k} \right) = \int d\vec{r} \ldots (\vec{r}) e^{-2j\vec{k} \cdot \vec{r}}, \tag{2}$$

and in the near field

$$E\left(\vec{k} \right) = \int d\vec{r} \ldots (\vec{r}) e^{-2jk\left| \vec{R} - \vec{r} \right|}, \tag{3}$$

where $E(\vec{r})$ is the measured electric field, $\vec{k}$ is the wave number vector, $\ldots(\vec{r})$ is the reflection coefficient of the electromagnetic wave at the point $\vec{r}$, $\vec{R}$ is the distance from antenna to an object. The far field condition is

$$R > 2D^2 \big/ \lambda \, , \qquad (4)$$

where D is the biggest dimension of an object, λ is the shortest wavelength.

Formula (2) is Fourier transformation, so this integral can be inverted, and we get ISAR image integral

$$\rho(\vec{r}) = \int d\vec{k} E(\vec{k}) e^{2 j \vec{k} \times \vec{r}} . \qquad (5)$$

Our measurements were performed in polar coordinates and the image was conveniently drawn in Cartesian coordinates

$$\rho(x, y) = \int_0^{2\pi} \int_{-\infty}^{\infty} E_\varphi(S) |S| e^{2 j S (x \cos(\varphi) + y \sin(\varphi))} dS d\varphi . \qquad (6)$$

Here we used polar coordinates by Jacobian $|S| \, dS$. This integral can be integrated simply by S considered it as Fourier integral. Digital signal filtration should be used in systems working within band 1 GHz–26 GHz, and finally we get image formula

$$\rho(x, y) = \int_0^{2\pi} E_\varphi' (x \cos(\varphi) + y \sin(\varphi)) d\varphi , \qquad (7)$$

where $E_\varphi'(t)$ – is electric field filtered with $|S|$ filter at the angles φ in the range of (0-360) degrees.

In the case of near-field, the final formula includes the distance to an object R

$$\rho(x, y) = \int_0^{2\pi} E_\varphi' (\sqrt{R^2 - R(x \cos(\varphi) + y \sin(\varphi)) + x^2 + y^2}) d\varphi . \qquad (8)$$

This integral can be transformed to summation using effective computational algorithms [11].

For ISAR imaging it was used improved near-field algorithm modified for time domain signals. It allows to avoid ghost artifacts that appear when far-field algorithm is employed for the same purpose.

III. EXPERIMENTAL SETUP

Our measurements of ISAR image creation were carried out by using UWB radar system inside a room where the ghost effects are possible. The scheme of the system together with the investigated object placed on the positioner is presented in Fig. 1.

The system includes generator 1 with short pulse former 2, the wideband transmitting 4 and receiving 7 double-ridged horns. The investigated object is placed on a rotating positioner 5. Part of the short pulse through directional coupler 3 as well as electrical signal from the horn 7 are fed to sampling head 8 and processed by sampling convertor 9. Useful information is sent to computer 14 through USB channel for further processing.

The distance between the antennas and the object was about 4 m. The duration of the elementary measurement was about 3 ns while the rotation period of the positioner is 3 minutes.
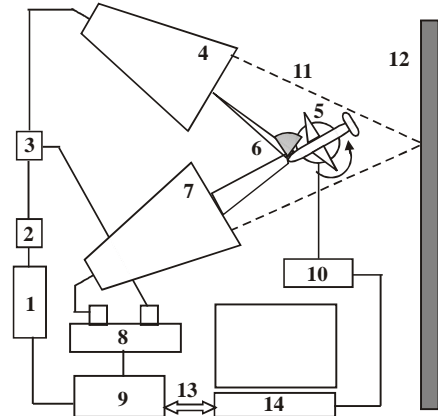

Fig. 1. Schematic diagram of indoor ISAR radar system measurements. 1 – pulse generator; 2 – short pulse former; 3 – directional coupler; 4 – the wideband transmitting horn; 5 – object under test; 6 – UWB pulse scattering from the object; 7 – the wideband receiving horn; 8 – sampling head; 9 – sampling converter; 10 – positioner control unit; 11 – parasitic reflection pulse; 12 – room wall; 13 – USB channel; 14 – computer with monitor.

The system works as follows. The pulse former of the generator forms short electrical pulse. Its spectrum and oscillogram are presented in Fig. 2.
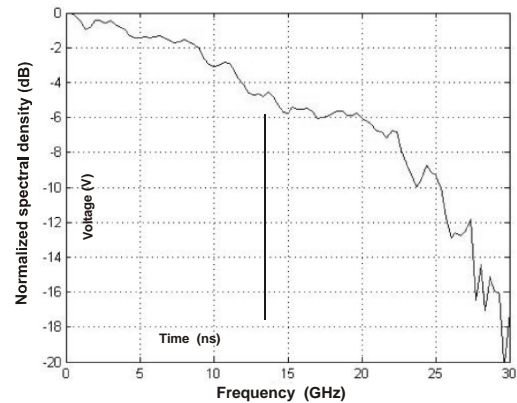

Fig. 2. Normalized spectral density of short electrical pulse generated by the system. In inset: the oscillogram of the pulse of the system.

The electrical pulse has duration of about 40 ps at half maximum and wide spectrum with $f_{up} = 22$ GHz at –10 dB. Parameter γ is equal to 0.956 what indicates UWB characteristic of the electrical pulse. This pulse feeds the horn 4 which radiates electromagnetic pulse.
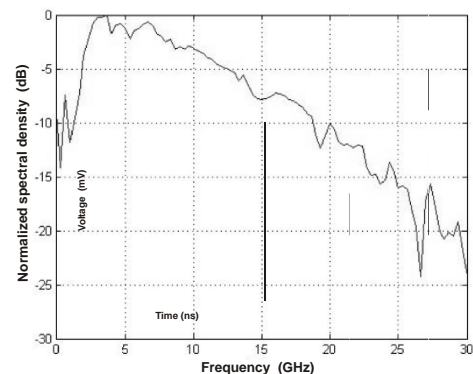

Fig. 3. Normalized spectral density of electromagnetic pulse formed by the radiating antenna (4) and directly received by the antenna (7). In inset: oscillogram of the pulse.

Fig. 3 presents spectrum and oscillogram of this electromagnetic pulse received by the horn 7 in the case when it is transmitted directly from the horn 4. Estimations of parameter у at the level of −10 dB give у = 0.897 what also indicates UWB characteristics of the electromagnetic pulse.

ISAR image is radar cross section (RCS) density image. Therefore calibration is necessary for correction of errors influenced by the system equipment. A well-known analytical solution of simple object like metal sphere was used for calibration [12]. Using the optimal filtration formula gives the calibrated electric field as

$$E\left(\vec{k}\right)=F\left(j\check{S}\right)\frac{F_T\left(j\check{S}\right)F_K^*\left(j\check{S}\right)}{\left|F_K\left(j\check{S}\right)\right|^2+\Gamma\max\left(\left|F_K\left(j\check{S}\right)\right|^2\right)},\quad(9)$$

where $F(j\ )$ is the spectrum of the pulse reflected from the target. $F_T(j\ )$ is theoretical frequency response, the square root of RCS of the calibration object (conducting sphere). $F_K(j\ )$ is the spectrum of the pulse reflected from the calibration target and $\ $ is optimal parameter empirically chosen to maximize signal to noise ratio.
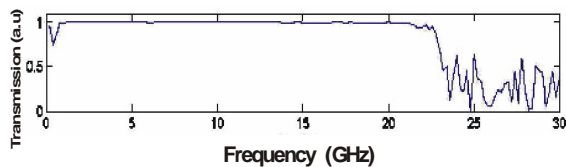

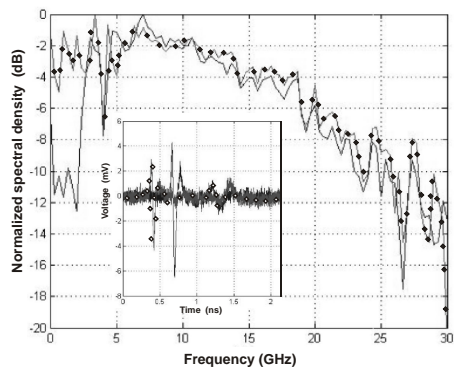Fig. 4. The transfer function of the UWB radar system.

Fig. 5. Normalized spectral densities of the two signals received at two different angles. In inset: oscillograms of the signals.
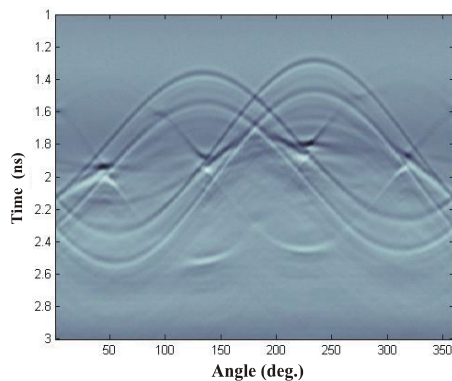

Fig. 6. Sinogram of the signals reflected from the object.

The following steps were taken to perform the procedure of calibration. First, theoretical frequency response of the

5 cm diameter sphere was calculated. Then, using the UWB system the spectrum of the impulse reflected from the sphere was measured. Next, we obtained a relation of these two frequency dependencies. Finally, as it is presented in Fig. 4, the transfer function of the system after the calibration is obtained. It is close to one up to 22 GHz.

The imaging signal is reflected from the rotating object and is detected periodically with a step of 1 degree (see Fig. 1). Figure 5 presents two spectra and two oscillograms corresponding to signals received from the object at two different angles. Reflection significantly decreases the voltage of the received signals but, however, the UWB characterization remains unchanged. Sinogram, i.e. the signals detected at all angles, is presented in Fig. 6. The vertical axis represents the duration of received pulses.

IV. THE IMAGES OBTAINED USING THE SYSTEM

To obtain high quality images with high resolution, the electromagnetic pulse envelope width (defined as width of analytic envelope at half maximum) should not exceed few hundred ps. That is confirmed for our system. As one can see from Fig. 3, the spectral frequency range at -20 dB of the radiated UWB signal is about 26 GHz which corresponds to the upper frequency of the sampling converter.

In Fig. 7 it is presented the image of metalized model plane obtained when testing the ISAR imaging system.
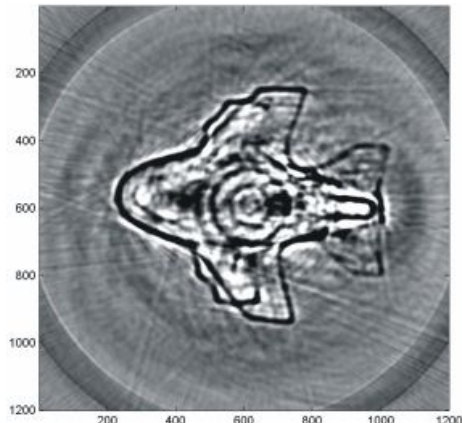

Fig. 7. ISAR image of model plane with metalized surface.

Microwave radiation is readily transmitted through most non-metallic media, thus enabling the microwave systems to "see" through concealing barriers such as packaging, wood, cardboard, clothing and others. Thus microwave systems can be used for detection and identification of concealed materials.

Figure 8 shows image of a spanner placed behind a wooden 4 cm-thick door. As one can see the object is easily identifiable.

It is known [13] that the spatial resolution improves by using shorter radiation wavelengths. For identification of small concealed objects the terahertz imaging is often used [13], [14]. Such terahertz radiation is strongly absorbed by water, so for detection of organic materials and passing moist barriers the microwave imaging is far more efficient. ISAR image of an apple is presented in Fig. 9. The structure of the apple depicted sufficiently well, with the distinguishable heart and peel.
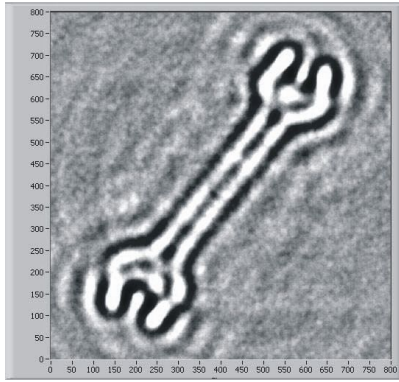
Fig. 8. ISAR image of spanner placed behind wooden door of 4 cm in thickness.
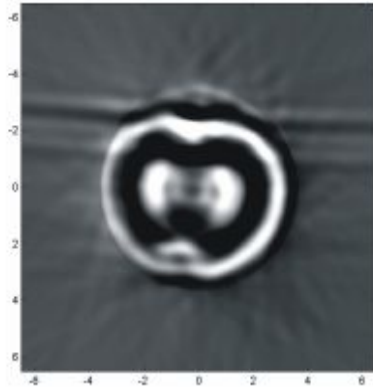

Fig. 9. ISAR image of an apple as organic object.

In practical applications the important characteristics are radiated power and sensitivity of receiver. Changing these two to fit required conditions is not complex in the case of microwaves, unlike the terahertz case which requires receiver cooling to increase the sensitivity and increasing of power level is complicated too. The cost of these imaging system components should be considered when mass production is of importance, in which case microwave imaging also becomes preferable.

The horn is excited by electrical pulse and radiates an EM pulse that is enriched by high frequency harmonics. This EM pulse spans into the frequency region which is higher than horn upper passband frequency determined by rigorous criteria. The received EM pulse has a shape of the differentiated exciting pulse (see insert in Fig. 3). This means that usage of radar components with shorter feeding pulse and receiver with higher upper frequency will make it possible to increase microwave spectra of such radar system with double-ridged horns up to 40 GHz–50 GHz. Wide band horns continue to be improved using both resistive layers and even meta materials [15], [16].

V. CONCLUSIONS

UWB pulses let overcome a lot of measurement problems: signal leakage through antennas, occasional reflection from the room walls and ceilings. Use of wideband double–ridged horns in UWB radar system allows to obtain high resolution images of different metallic and organic objects as well as of objects placed behind various obstacles. The employed improved near-field algorithm assists in obtaining ISAR images of good quality. The process of image construction revealed that improvement of corresponding elements of the system, such as shortening of the forming pulse, widening of frequency band of the receiver horn and sampling converter, allows using microwave imaging in range having upper frequency 40 GHz–50 GHz.

VI. ACKNOWLEDGEMENTS

REFERENCES

[1] M. Bimpas, K. Nikellis, N. Paraskevopoulos, D. Econonou, N. Uzunoglu, "Development and testing of a detector system for trapped humans in building ruins", *33rd European Microwave Conf.*, 2003, vol. 3, pp. 999–1002.

[2] A. G Jarovoy, L. P. Lighart, J. Matuzas, B. Levitas, "UWB radar for human being detection", *IEEE Aerospace and Electronic Systems*, vol. 21, no 3, pp. 10–14, 2006. [Online]. Available: http://dx.doi.org/10.1109/MAES.2006.1624185

[3] L. Jofre, A. Broquetas, J. Romeu, S. Blanch, A. P. Toda, X. Fabregas, A. Cardama, "UWB Tomographic radar imaging of penetrable and impenetrable objects", in *Proc. IEEE*, 2009, pp. 451–464. [Online]. Available: http://dx.doi.org/10.1109/JPROC.2008.2008854

[4] S. Asmontas, A. Laurinavicius, J. Paukste, A. Silenas, "Microwave radiation and X-ray induced phenomena in semiconductors", *Lith. J. Physics,* vol. 45, no. 6, pp. 423–436, 2005. [Online]. Available: http://dx.doi.org/10.3952/lithjphys.45606

[5] S. Asmontas, F. Anisimovas, L. Dapkus, J. Gradauskas, O. Kiprijanovic, I. Prosycevas, J. Puiso, K. Slapikas, B. Vengalis, "Radiation of ultra-wideband electromagnetic pulses by pulsed excitation of rectangular antenna", *Lith. J. Physics,* vol. 49, no. 1, pp. 29–34, 2009. [Online]. Available: http://dx.doi.org/10.3952/lithjphys.49105

[6] W. G. Carrara, R. S. Goodman, R. M. Majewski, *Spotlight Synthetic Aperture Radar – signal processing algorithms.* Artech House: Boston, 1995.

[7] B. Levitas, J. Matuzas, "Evaluation of UWB ISAR image resolution", in *Proc. European Radar Conf.*, 2005, pp. 89–91.

[8] V. Kravchenko, O. Lazorenko, V. Pustovoit, L. F. Chernogor, "A new class of fractal ultra-wideband signals", *Doklady Physics*, vol. 52, no. 3, pp. 129–133, 2007. [Online]. Available: http://dx.doi.org/10.1134/S1028335807030019

[9] F. Anisimovas, S. Asmontas, O. Kiprijanovic, J. Matuzas, "Radiation of large bandwidth and long duration signals by pulsed excitation of monopole antennas", in *Proc. 4th Intern. Conf. Radiation Interaction with Material and its Use in Technologies*, Kaunas, Lithuania, 2012, pp. 574–577.

[10] F. F. Dubrovka, G. A. Yena, P. Y. Stepanenko, V. M. Tereschenko, "Ultra wideband double ridged horns with rectangular aperture", in *Conf. Rec. IEEE Int. Conf. Antenna theory and Techniques,* Sevastopol, Ukraine, 2003, pp. 590–593.

[11] V. Chen, H. Ling, *Time-Frequency Transforms for Radar Imaging and Signal Analysis.* Boston-London: Artech House, 2002.

[12] A. Stratton, *Electromagnetic Theory.* New York, London: McGraw-Hill Book Company, Inc., 1953.

[13] J. F. Federki, B. Schulkin, F. Huang, D. Gary, R. Barat, F. Oliveira, D. Zimdars, "THz imaging and sensing for security applications – explosives, weapons and drugs", *Semicond. Sci Technol.,* vol. 20, pp. S266–S280, 2005. [Online]. Available: http://dx.doi.org/10.1088/0268-1242/20/7/018

[14] L. Minkevicius, V. Tamosiunas, I. Kasalynas, D. Seliuta, G. Valusis, A. Lisauskas, S. Boppel, H. G. Roskos, K. Kohler, "Terahertz heterodyne imaging with InGaAs-based bow-tie diode", *Applied Physics Letters,* vol. 99, p. 131101, 2011. [Online]. Available: http://dx.doi.org/10.1063/1.3641907

[15] B. Jacobs, J. W. Odendaal, J. Joubert, "An improved design for a 1-18 GHz double-ridged guide horn antenna", *IEEE Trans. Antennas and Propagation*, vol. 60, no. 9, pp. 4110–4118, 2012. [Online]. Available: http://dx.doi.org/10.1109/TAP.2012.2207043

[16] D. Ramaccia, F. Scattone, F. Bilotti, A. Toscano, "Broadband compact horn antennas by using EPS-ENZ metamaterial lens", *IEEE Trans. Antennas and Propagation*, vol. 61, no. 6, pp. 2929–29, 2013. [Online]. Available: http://dx.doi.org/10.1109/TAP.2013.2250235